Uniform Nanozeolite Microspheres with Large Secondary Pore Architecture

Yijin Kang,† Wei Shan,† Jingyi Wu,† Yahong Zhang,*,† Xiaoyan Wang,† Wuli Yang,‡ and Yi Tang*,†

Department of Chemistry and Shanghai Key Laboratory of Molecular Catalysis and Innovative Materials, Fudan University, Shanghai 200433, People's Republic of China, and Department of Macromolecular Science and Key Laboratory of Molecular Engineering of Polymers (Minister of Education), Fudan University, Shanghai 200433, People's Republic of China

Received January 12, 2006. Revised Manuscript Received February 6, 2006

Various nanozeolites microspheres with uniform diameters from 3 to 8 μm were prepared by a polymerization-induced colloid aggregation method. The obtained nanozeolite microspheres possess a regularly spherical morphology and a large and adjustable secondary pore architecture that are believed to be useful in the separation of biomolecules. Moreover, the nanozeolite microspheres well retain the properties of the original colloidal nanozeolites and exhibit similar advantages to those of zeolite nanoparticles in protein adsorption. More importantly, the large secondary pore size (15−70 nm) of nanozeolite microspheres has been proven to have little limiting effect on the adsorption rate of various proteins, and a saturated adsorption is achieved even within 10 min, which may also facilitate microspheres' applications in catalysis involving diffusion limitations.

1. Introduction

Because of the combination of the shape-selectivity of micropores, acid catalytic activity, and thermal/hydrothermal stability, zeolites have been widely used as heterogeneous catalysts and adsorbents in the field of oil refining and in the petrochemical industry.[1] In the past decade, nanosized zeolites have attracted considerable attention[2,3] because of their potential advantages in both the solution of diffusion problems in catalysis involving large molecules and the preparation of zeolitic structured materials with a hierarchical porosity. Recently, a series of characteristic surface properties of nanozeolites was explored in our group, such as a large external surface area, tunable surface charges, abundant exposed active sites, and a high self-dispensability in both aqueous and organic solutions, which may open up possibilities for some unconventional applications, especially those involving biomacromolecules. For example, zeolite nanocrystals have been applied to enrich and directly identify trace peptides and proteins by matrix-assisted laser desorption ionization−time-of-flight mass spectrometry[4] as well as to immobilize enzymes for use in biosensors because of their large adsorption capacity and proper interactions with proteins and enzymes.[5] In addition, through a uniform outer-surface grafting, metal-ion-immobilized zeolite β nanoparticles could further be used to isolate and identify phosphopeptides from protein digests.[6] Moreover, the thermal, acidic/alkaline, and attrition stabilities of zeolite materials would allow them to be applied under some severe conditions.[7] However, in many practical bioapplications such as chromatographic separation, the nanozeolites cannot be directly used because of their small size and, consequently, a high-pressure drop; although, Sakaguchi et al.[7a] have predicted that zeolite materials should be much better chromatographic carriers than the hybrid silica. To overcome this problem, we have electrostatically adsorbed nanozeolites on the surface of disklike diatomites and found that the Co^{2+}-exchanged nanozeolite/diatomite composite could be used as an affinity-chromatographic stationary phase to separate the histidine-containing peptides.[8] As a perfect chromatographic carrier, however, a spherical morphology with a uniform size (usually on the micrometer scale) is more preferred for the sake of

* Authors to whom correspondence should be addressed. E-mail: zhangyh@fudan.edu.cn (Y.Z.), yitang@fudan.edu.cn (Y.T.). Tel.: 86-21-55664125. Fax: 86-21-65641740.

† Department of Chemistry and Shanghai Key Laboratory of Molecular Catalysis and Innovative Materials.

‡ Department of Macromolecular Science and Key Laboratory of Molecular Engineering of Polymers.

(1) (a) Rolison, D. R. *Chem. Rev.* **1990**, *90*, 867. (b) Cundy, C. S.; Cox, P. A. *Chem. Rev.* **2003**, *103*, 663. (c) Weitkamp, J. *Solid State Ionics* **2000**, *131*, 175.

(2) (a) Tosheva, L.; Valtchev, V. P. *Chem. Mater.* **2005**, *17*, 2494. (b) Smaihi, M.; Gavilan, E.; Durand, J.-O.; Valtchev, V. P. *J. Mater. Chem.* **2004**, *14*, 1347.

(3) (a) Valtchev, V. P.; Mintova, S. *Microporous Mesoporous Mater.* **2001**, *43*, 41. (b) Holland, B. T.; Abrams, L.; Stein, A. *J. Am. Chem. Soc.* **1999**, *121*, 4308. (c) Rhodes, K. H.; Davis, S. A.; Caruso, F.; Zhang, B.; Mann, S. *Chem. Mater.* **2000**, *12*, 2832. (d) Dong, A.; Wang, Y.; Tang, Y.; Zhang, Y.; Ren, N.; Gao, Z. *Adv. Mater.* **2002**, *14*, 1506. (e) Huang, L.; Wang, Z.; Sun, J.; Miao, L.; Li, Q.; Yan, Y.; Zhao, D. *J. Am. Chem. Soc.* **2000**, *122*, 3530. (f) Zhang, B.; Davis, S. A.; Mann, S. *Chem. Mater.* **2002**, *14*, 1369.

(4) Zhang, Y. H.; Wang, X. Y.; Shan, W.; Wu, B. Y.; Fan, H. Z.; Yu, X. J.; Tang, Y.; Yang, P. Y. *Angew. Chem., Int. Ed.* **2005**, *44*, 615.

(5) Yu, T.; Zhang, Y. H.; You, C. P.; Zhuang, J. H.; Wang, B.; Liu, B. H.; Kang, Y. J.; Tang, Y. *Chem.—Eur. J.* **2006**, *12*, 1137.

(6) Zhang, Y. H.; Yu, X. J.; Wang, X. Y.; Shan, W.; Yang, P. Y.; Tang, Y. *Chem. Commun.* **2004**, 2882.

(7) (a) Matsui, M.; Kiyozumi, Y.; Yamamoto, T.; Mizushina, Y.; Mizukami, F.; Sakaguchi, K. *Chem.—Eur. J.* **2001**, *7*, 1555. (b) Sakaguchi, K.; Matsui, M.; Mizukami, F. *Appl. Microbiol. Biotechnol.* **2005**, *67*, 306.

(8) Xu, F.; Wang, Y. J.; Wang, X. D.; Zhang, Y. H.; Tang, Y.; Yang, P. Y. *Adv. Mater.* **2003**, *15*, 1751.

10.1021/cm060084w CCC: $33.50
Published on Web 03/14/2006

obtaining a homogeneous, rapid adsorption and desorption behavior. Recently, some micrometer-sized hollow zeolite spheres have been fabricated through adsorbing the zeolite nanocrystals onto the removable spherical hard templates.[9] However, the mechanical strength of the obtained materials was too low for most practical applications. Although the secondary hydrothermal treatment could improve their mechanical strength,[10] the characteristics of nanozeolites would be lost because of the growth of the zeolite crystals. For the purpose of optimizing the catalytic performance and the convenience of handling, Sterte and co-workers[11] first prepared mesoporous solid zeolite spheres with a diameter of several-hundred micrometers by in situ crystallization of the colloidal precursor of zeolites containing the macroporous anion-exchange resin beads. In this paper, a universal and simple processing method called polymerization-induced colloid aggregation (PICA)[12] is first employed to prepare nanozeolite microspheres with various compositions and uniform diameters of 3−8 μm, which well match the optimum size for most chromatographic applications. The as-synthesized nanozeolite microspheres feature a uniform spherical morphology and a large and adjustable secondary pore architecture. More importantly, the polymeric shaping process from dispersed zeolite nanoparticles to nanozeolite microspheres well maintained the characteristic properties of colloidal nanozeolite crystals, such as a high adsorption capacity and a rapid adsorption rate for proteins even with high molecular weights, which are expected to be useful in the adsorption and separation of proteins with a wide range of molecular weights.

2. Experimental Section

2.1. Materials. Formaldehyde (38 wt %), urea, hydrochloric acid (36 wt %), and ethanol were obtained from Shanghai Chemical Reagent Company. Lysozyme (14.3 kDa), ovalbumin (43 kDa), and ferritin (440 kDa) were purchased from Aldrich. All of the chemicals were directly used without further purification. Zeolite nanocrystals (β, ZSM-5, and silicalite-1) were hydrothermally synthesized according to previous reports.[13] The particle size and crystalline structure of the nanozeolites were determined by scanning electron microscopy (SEM) and X-ray diffraction (XRD).

2.2. Fabrication of Nanozeolite Microspheres. The typical synthesis process of nanozeolite microspheres was as follows. A total of 1.1 g of a 100 mg g^{-1} zeolite nanocrystals suspension was added to 4 mL of distilled water. Then, 0.38 g of ethanol, 0.34 g of urea, and 50 μL of a HCl solution (36 wt %) were added in sequence, and the resultant mixture was stirred until the urea was completely dissolved. Afterward, 384 μL of a formaldehyde solution (38 wt %) was added under stirring, and a white precipitate was generated within several seconds. After being statically placed at ambient temperature (ca. 25 °C) for 1 h, the product was recovered by filtration, washed with distilled water and ethanol, and dried at 60 °C. Finally, the sample was calcined in air at 700 °C for 3 h with a heating rate of 1 °C min^{-1} to remove the urea−formaldehyde polymer and the organic templates in the nanozeolites.

2.3. Adsorption and Adsorbing Dynamics Processes of Proteins in Nanozeolite Microspheres. *2.3.1. Experiment of Adsorbing Proteins (Ferritin, Ovalbumin, and Lysozyme).* A total of 2.0 mg of nanozeolite microspheres was dispersed in 1.0 mL of a 20 mM phosphate buffer solution (PBS) containing 1.0 mg mL^{-1} of protein at different pH values (from pH 2 to 12) and kept in a water bath at 37 °C for 1 h. The adsorption amount of the proteins was obtained through measuring the UV absorbance of the protein solution at $\lambda = 280$ nm before and after adsorption. For comparison, the adsorption behavior of zeolite nanocrystals for proteins was also determined as follows. A total of 10 μL of a 10 mg mL^{-1} nanozeolite suspension was dispersed in 0.5 mL of PBS containing a 0.1 mg mL^{-1} protein solution at different pH values and kept in a water bath at 37 °C for 1 h. The adsorption amounts of the proteins at different pH values were measured by the method mentioned above. To accurately calculate the adsorption amount, a calibration curve was created by using a series of protein solutions with different concentrations in 20 mM PBS at pH 7.0 before measurement.

2.3.2. Experiment of Adsorbing Dynamics of Proteins. A total of 2.0 mg of nanozeolite microspheres was dispersed in 1.0 mL of a 1.0 mg mL^{-1} protein solution buffered at pH 8 for lysozyme adsorption and pH 5 for ferritin adsorption, respectively, and kept in a water bath at 37 °C for 2, 10, 20, 30, 50, 80, and 120 min. The adsorption amount of the protein at different adsorption times was obtained through measuring the UV absorbance of the protein solution at $\lambda = 280$ nm as mentioned above.

2.4. Characterization. SEM and transmission electron microscopic (TEM) studies of nanozeolite microspheres were performed on Philips XL 30 and JEOL 200 apparatuses with accelerated voltages of 20 and 200 kV, respectively. The thermogravimetric and differential thermal analysis (TG−DTA) of the samples was performed on an SII TG/DTA 6200 apparatus from room temperature to 800 °C at a heating rate of 1 °C min^{-1} in the air. The N_2 sorption isotherms of the samples were measured by using a Micromeritics TriStar 3000 system at liquid-nitrogen temperature. The crystalline type of zeolites was characterized by XRD on a Rigaku D/max-IIA diffractometer with Cu Kα radiation at 40 kV and 20 mA. The UV absorbance of the protein solution was recorded on a Shimadzu UV-2450 spectrophotometer.

3. Results and Discussion

3.1. Fabrication of Nanozeolite Microspheres. Figure 1 shows the SEM images of the zeolite nanocrystals employed in this paper. All of the samples exhibit a good monodispersity, and the mean sizes of zeolites β (80), β (50), silicalite-1 (80), and ZSM-5 (150) are 80, 50, 80, and 150 nm, respectively. Figure 2a is the SEM image of the nanozeolite β−polymer hybrid microspheres fabricated from nanozeolite β (80) under the typical synthesis process. It was found that the product could be recovered in 1 h and possesses a regularly spherical morphology with a very uniform diameter of 7 μm and a rather smooth surface. The

(9) (a) Wang, X. D.; Yang, W. L.; Tang, Y.; Wang, Y. J.; Fu, S. K.; Gao, Z. *Chem. Commun.* **2000**, 2161. (b) Rhodes, K. H.; Davis, S. A.; Caruso, F.; Zhang, B.; Mann, S. *Chem. Mater.* **2000**, *12*, 2832.
(10) (a) Valtchev, V. *Chem. Mater.* **2002**, *14*, 956. (b) Valtchev, V. *Chem. Mater.* **2002**, *14*, 4371.
(11) (a) Tosheva, L.; Valtchev, V.; Sterte, J. *Microporous Mesoporous Mater.* **2000**, *35*−*36*, 621. (b) Tosheva, L.; Mihailova, B.; Valtchev, V.; Sterte, J. *Microporous Mesoporous Mater.* **2001**, *48*, 31. (c) Naydenov, V.; Tosheva, L.; Sterte, J. *Microporous Mesoporous Mater.* **2002**, *55*, 253. (d) Naydenov, V.; Tosheva, L.; Sterte, J. *Chem. Mater.* **2002**, *14*, 4881.
(12) (a) Jiang, Z. T.; Zuo, Y. M. *Anal. Chem.* **2001**, 73, 686. (b) Kirkland, J. J. U.S. Patent 3,782,075, Jan 1, 1974. (c) Unger, K. K. *Porous Silica*; Elsevier Press: New York, 1979; Chapter 2.
(13) (a) Camblor, M. A.; Corma, A.; Mifsud, A.; Perez-Pariente, J.; Valencia, S. *Stud. Surf. Sci. Catal.* **1997**, *105*, 34. (b) Persson, A. E.; Schoeman, B. J.; Sterte, J.; Ottesstedt, J.-E. *Zeolites* **1994**, *14*, 557. (c) Persson, A. E.; Schoeman, B. J.; Sterte, J.; Ottesstedt, J.-E. *Zeolites* **1994**, *15*, 611.

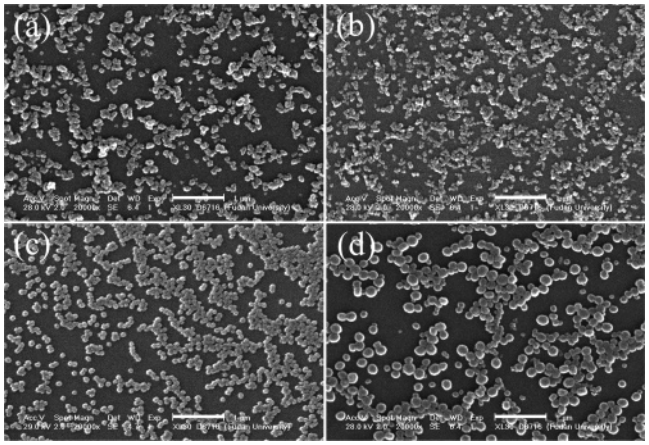

Figure 1. SEM images of (a) zeolite β (80), (b) β (50), (c) silicalite-1 (80), and (d) ZSM-5 (150). The scale bars are 1 μm.

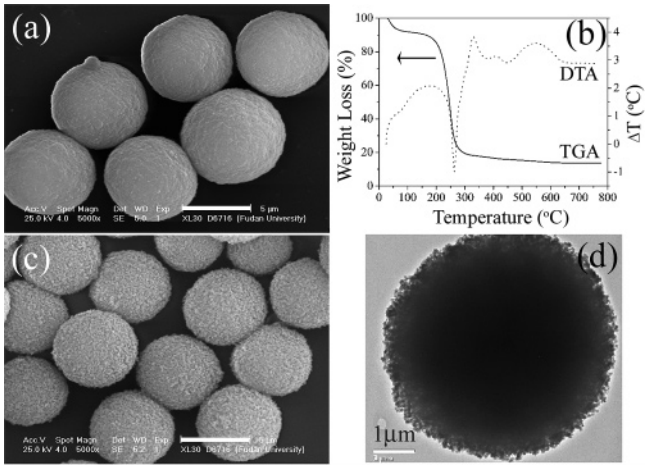

Figure 2. SEM image (a) and TG-DTA curves (b) of the nanozeolite−polymer hybrid microspheres obtained from zeolite β (80). SEM (c) and TEM (d) images of the nanozeolite β (80) microspheres obtained by calcining the nanozeolite−polymer hybrid microspheres in part a. The scale bars in the SEM images are 5 μm.

prolonging of the reaction time has little influence on the morphology of the product. The TG−DTA plot (Figure 2b) of the prepared nanozeolite β (80)−polymer hybrid microspheres in air has three weight-loss steps. The first one, appearing below 100 °C, could be assigned to the desorption of water. The second steep step, accompanied by a large endothermic peak between 200 and 280 °C, could be attributed to the combustion/pyrolysis of the urea−formaldehyde polymer, while the third smooth step between 350 and 650 °C may correspond to the decomposition of organic species or templates in the micropores of nanozeolite. There was no weight loss above 650 °C, indicating that the polymer and organic template in the hybrid microspheres have been completely removed below this temperature. Figure 2c shows the product after completely removing the polymer and organic template. The resultant nanozeolite microspheres well retained the regularly spherical morphology of the original hybrid microspheres except for a small shrinkage of diameter from 7 to 6.3 μm. Because of the removal of the organic component, the zeolite nanoparticles could be clearly observed on the surface of the calcined microspheres (Figure 2c). The TEM image (Figure 2d) clearly indicates that the obtained microspheres are composed of interlinked nanozeolite particles, which self-support the intact spherical morphology of the product. Furthermore, the 3D-connected large mesoporosity between the nanozeolite particles could also be clearly distinguished on the peripheral zone of the microspheres. More importantly, the product exhibited a good mechanical stability. No damage or collapse of the nanozeolite microspheres could be observed even under a rigorous ultrasonication for about 30 min.

The N_2 sorption isotherms of nanozeolitite β (80) microspheres are shown in Figure 3a. A large hysteresis loop is observed at a high relative pressure (p/p_0), revealing the presence of large mesopores in the nanozeolite β microspheres. The total Brunauer−Emmett−Teller surface area of the product is 578 $m^2\ g^{-1}$, while the micropore area and external surface area (t plot) are 414 $m^2\ g^{-1}$ and 164 $m^2\ g^{-1}$, respectively, indicating that the nanozeolite component is well-crystallized and has an abundant exposed surface area. The pore diameter distribution curve derived from the Barret−Joyner−Halenda (BJH) model displays a clear secondary porosity with a diameter ranging from 20 to 75 nm (Figure 3a, inset), which is believed to be advantageous for the adsorption and separation of large biomolecules. The XRD pattern of the nanozeolite microspheres proves the crystalline structure of zeolite β (Figure 3b).

Two factors were found to be important for the fabrication of nanozeolite microspheres. One is the content of the nanozeolite particles in the initial synthesis solution, which greatly influences the morphology of the final product. Figure 4A displays the relationship between the nanozeolite content in the original synthesis solution and the diameters of

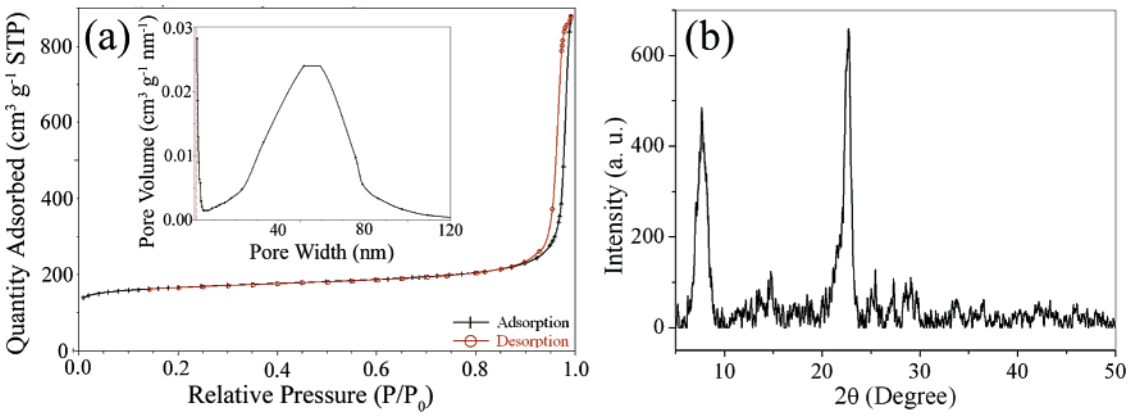

Figure 3. N_2 sorption isotherms (a), pore diameter distribution (a, inset), and XRD pattern (b) of the nanozeolite β (80) microspheres.

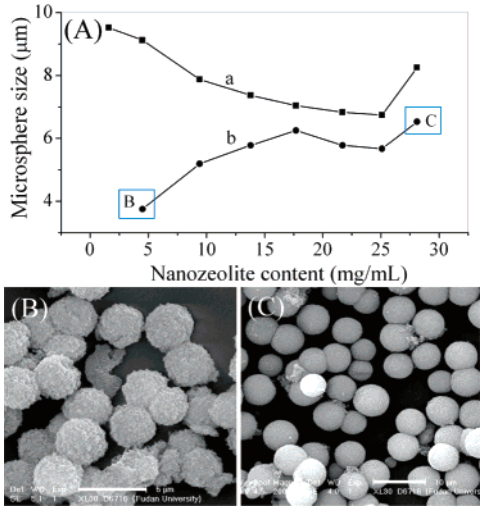

Figure 4. Relationship (A) of the sizes of nanozeolite β (80) microspheres before (a) and after (b) calcination with the content of nanozeolite in the original synthesis solution. Parts B and C represent the typical SEM images of the samples corresponding to points B and C on curve b, respectively. The scale bars in B and C are 5 and 10 μm, respectively.

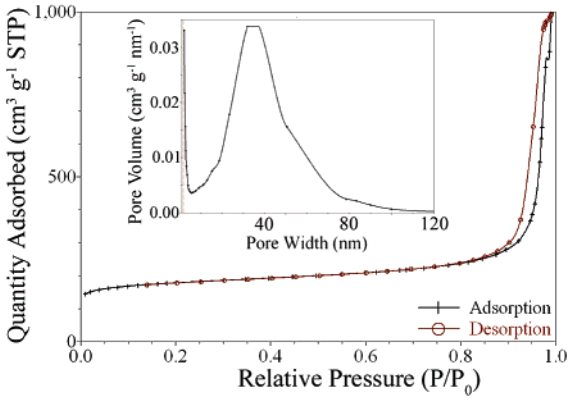

Figure 5. N_2 sorption isotherms and pore diameter distribution (inset) of the nanozeolite β (50) microspheres.

nanozeolite microspheres before and after removing the polymer. Obviously, both of the sizes and the shrinkage ratios during calcination of nanozeolite microspheres vary with the content of nanozeolites in the initial synthesis system. When the nanozeolite content is lower than 10 mg mL^{-1}, the amount of nanozeolite incorporated into the hybrid microspheres is insufficient to support their spherical structure, which leads to a remarkable shrinkage and even a collapse of their spherical morphology after calcination (Figure 4B). In contrast, if the content of nanozeolite exceeds 25 mg mL^{-1}, the size of the nanozeolite microspheres would abruptly increase, and the nanozeolite particles cannot be completely incorporated into the composite microspheres during the urea−formaldehyde polymerization. Some residual zeolite nanocrystals were clearly observed in the final product (Figure 4C). When the content of nanozeolites in the original synthesis solution is between 10 and 25 mg mL^{-1}, the spherical morphology of the product could be well retained after calcinations. Moreover, with the increasing content of nanozeolites in the synthesis solution, the shrinkage ratios of the product during calcination decrease while their compact degree and mechanical stability increase. The product with the smallest shrinkage ratio and the highest mechanical stability was obtained at the nanozeolite content of 17 mg mL^{-1} (Figure 2c). The second key factor for the fabrication of nanozeolite microspheres is the size of the zeolite nanoparticles, which determines the secondary pore size of the final product. For example, when the size of zeolite β nanocrystals decreased from 80 nm (Figure 1a) to 50 nm (Figure 1b), the most probable secondary pore diameter of the product decreased from 51.9 nm (Figure 3a, inset) to 31.7 nm (Figure 5, inset). Because the mesoporous structure in the final nanozeolite microspheres is resulted from the accumulation of the nanozeolite particles, we could easily adjust it via employing nanozeolite particles with different sizes.

Besides, the acidity of the initial solution could also affect the formation of nanozeolite microsphere. Generally, the size of nanozeolite microspheres decreases with the increasing acidity of the synthesis solution. The polymerization of urea−formaldehyde can be catalyzed by acid,[14] and thereby, a higher degree of acidity would lead to a high polymerization rate. As a result, with increasing acidity, the number of hybrid microspheres increases, but their size decreases. However, an excessively high acidity would lead to the separation of nanozeolites from polymers in the product because of the extremely fast polymerization rate, whereas too low of an acidity would cause the incomplete polymerization of urea−formaldehyde. Therefore, taking the size and morphology of nanozeolite microspheres into consideration, the appropriate acidity, that is, the amount of HCl solution (36 wt %) added in the synthesis solution, is in the range from 10 to 40 μL mL^{-1}.

This approach is also applicable to other types of nanozeolites with medium or high Si/Al ratios, such as silicalite-1 (Figure 1c) and ZSM-5 (Figure 1d). The products obtained by the aforementioned typical synthesis process are shown in Figure 6B and C. The corresponding particle size, surface area, pore volume, and secondary pore diameter distribution of various nanozeolite microspheres are listed in Table 1. Their crystalline structures are proved by their XRD patterns (Figure 6D). It is clear that their textural properties depend on both the type and the size of zeolite nanocrystals. The influence of the type of nanozeolites on the size of the final product may be attributed to the different surface properties of various nanozeolites (Figure 6 and Table 1).

3.2. Adsorption of Proteins in Nanozeolite Microspheres. As it has been pointed out, nanozeolite crystals have been suggested as promising candidates for the enrichment and immobilization of proteins and enzymes because of their large external surface area and adjustable surface properties.[4,5] However, in most of the applications, a shaping process is desired to assemble the zeolite nanocrystals into the aggregates without losing their original characteristics. To reveal the influences of such a shaping process on the properties of nanozeolite crystals, herein, three proteins with different molecular weights and sizes, lysozyme (14.3 kDa), ovalbumin (43 kDa), and ferritin (440 kDa), were selected as model proteins to study the protein adsorption behavior of the synthesized nanozeolite microspheres.

Figure 7a shows the adsorption amounts of three proteins in nanozeolite β (80) microspheres under different pH values.

(14) Liu, G. Q.; Yu, Z. L. *Chromatography Column Technique*; Chemical Industry Press: Beijing, 2002; Chapter 4.

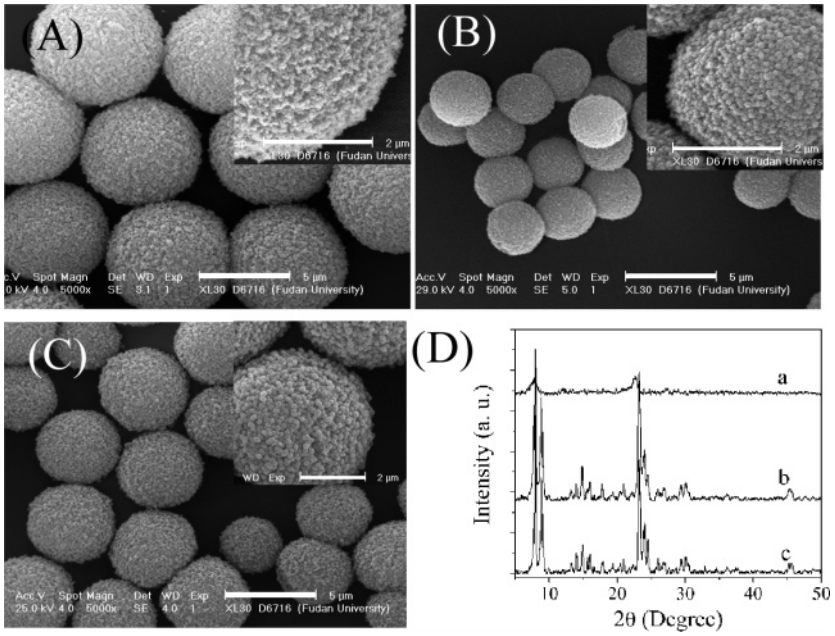

Figure 6. SEM images of nanozeolite microspheres derived from zeolite β (50) (A), silicalite-1 (B), and ZSM-5 (C) nanoparticles and their XRD patterns (D). The three XRD patterns in D correspond to the nanozeolite microspheres of zeolite β (50) (a), silicalite-1 (b), and ZSM-5 (c), respectively. The scale bars in the SEM images and their insets are 5 and 2 μm, respectively.

Table 1. Textural Properties of Various Nanozeolite Microspheres

nanozeolite type (size /nm)	$D_{\text{microsphere}}{}^{a}$ /μm	$D_{\text{secondarypore}}{}^{b}$ /nm	$A_{\text{micropore}}{}^{c}$ /m^2 g^{-1}	$A_{\text{externalsurface}}{}^{c}$ /m^2 g^{-1}	$V_{\text{micropore}}{}^{d}$ /cm^3 g^{-1}	$V_{\text{mesopore}}{}^{d}$ /cm^3 g^{-1}
β (80)	6.3	51.9	414.9	164.6	0.18	1.17
β (50)	5.8	31.7	401.8	218.9	0.18	1.37
silicalite-1 (80)	3.3	40	321.7	174.5	0.14	0.68
ZSM-5 (150)	5.0	75	251.6	172.6	0.11	0.45

[a] Diameter of nanozeolite microsphere. [b] Most probable diameter of the secondary pore in nanozeolite microsphere. [c] Micropore area and external surface area of nanozeolite microsphere calculated by t-plot method. [d] Micropore and mesopore volumes of nanozeolite microspheres obtained by t-plot method and desorption data using BJH model between 1.7 and 300 nm width, respectively.

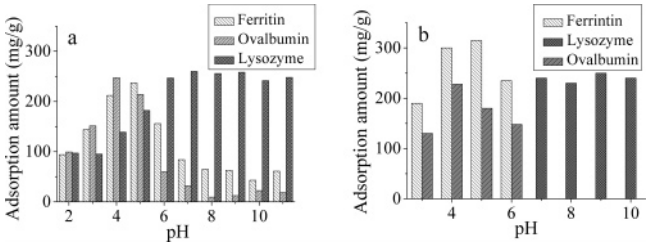

Figure 7. Adsorption amount of three model proteins with different molecular weights in the nanozeolite β (80) microspheres (a) and on the dispersed zeolite β (80) nanoparticles (b) under different pH values. The protein/nanozeolite ratio during adsorption is 0.5 (w/w).

Obviously, the nanozeolite microspheres display different adsorption behaviors for the different proteins. Similar to the dispersed zeolite nanocrystals (Figure 7b), nanozeolite microspheres have a large adsorption capacity under acidic conditions for the proteins with a lower isoelectric point (pI) (e.g., ovalbumin, pI = 4.6; ferritin, pI = 4.5), while the remarkable adsorption of proteins with a higher pI (e.g., lysozyme, pI = 11.0) occurs in a wide pH range. This phenomenon could be explained by the interaction of the positively charged proteins (at a pH below their pI) and the negatively charged surface of nanozeolites, which could help proteins to be adsorbed on the nanozeolites via electrostatic attraction.[7] When the pH of the solution is above the pI of the proteins, the proteins will carry a negative charge, which would prevent the protein's adsorption on the nanozeolites because of electrostatic repulsion. The proteins with a lower pI only have net positive charges under acidic conditions, whereas the proteins with a higher pI have a positive charge in a wide pH range. Therefore, two different adsorption behaviors were observed according to the pI values of the proteins. More notably, for the proteins with a relatively low molecular weight (or volume), the hierarchically structured nanozeolite microspheres possess a similar protein adsorption amount to that of the dispersed zeolite nanocrystals (Figure 6b), implying that this shape-processing process hardly influences the adsorbing performance of the nanozeolites; that is, the secondary pore formed during the shape processing is large enough for the accommodation of proteins with a relatively small size. However, for the protein with a very large size (e.g., ferritin), its adsorption amount in nanozeolite microspheres (Figure 7a) is a little lower than that in the colloidal zeolite nanocrystals probably because of the spatial limitation of the secondary pore (Figure 7b).

To give a comprehensive picture for the effect of the shaping process on the protein adsorption behaviors on the nanozeolite microspheres, the adsorbing dynamics of two typical proteins in nanozeolite β (50) microspheres were further investigated. Figure 8 displays the adsorption amount curves of lysozyme (14.3 kDa) at pH 8 and ferritin (440 kDa) at pH 5 in the nanozeolite β (50) microspheres. Both of the proteins present an amazing adsorption rate in the nanozeolite microspheres even if the nanozeolite micro-

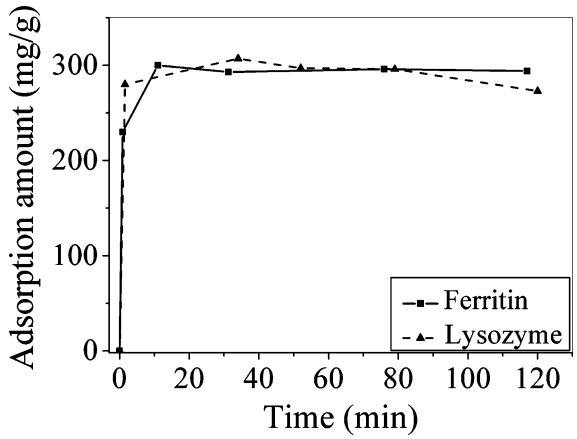

Figure 8. Adsorption amounts of lysozyme at pH 8 and ferritin at pH 5 in the nanozeolite β (50) microspheres as a function of time. The protein/nanozeolite ratio during adsorption is 0.5 (w/w).

spheres with a relatively smaller secondary pore size (31.7 nm) were used here. Almost 90% of the proteins can be adsorbed into nanozeolite microspheres in less than 2 min, and a saturated adsorption was achieved within 10 min. Such a rapid adsorption rate is similar to that on the dispersed zeolite nanocrystals, indicating that the space structure of nanozeolite microspheres has little limiting effect on the diffusion of proteins. These facts imply that the polymeric shaping process for the fabrication of nanozeolite microspheres has little influence on the properties of the original nanozeolite crystals, which ensures the inheritance of the outstanding proteins' and enzymes' adsorption performance of the nanozeolite crystals for the final nanozeolite microspheres.

4. Conclusions

In conclusion, various types of dispersed zeolite nanocrystals have been assembled into uniform nanozeolite microspheres with a secondary porosity through a PICA method. The obtained nanozeolite microspheres feature a uniform spherical morphology and a large and adjustable secondary pore architecture. They provide the greatest degree of retainment for the properties of the original nanozeolites and thereby have a protein adsorption amount similar to that of the dispersed nanozeolites. Furthermore, the open pore structure of the nanozeolite microspheres, that is, the large diameter of the secondary pore (larger than 30 nm), leads to a rapid adsorption rate for proteins with a wide range of molecular weights from 14 to 440 kDa, which would provide a new material for the separation and immobilization of various proteins. Additionally, the nanozeolite microspheres are also believed to find their applications in catalysis involving diffusion limitations owing to their uniform spherical morphology and abundant secondary porosity.

Acknowledgment. This work was supported by the NSFC (20303003, 20421303, 20473022, 20325313, and 20233030), the STCSM (05XD14002, 05QMX1403, and 05DJ14005), the Major State Basic Research Development Program (2003CB615807), and the Key Science Research Fund of the Ministry of Education.

CM060084W